In situ high-pressure study of ammonia borane by Raman and IR spectroscopy

Shuntai Xie, Yang Song, and Zhenxian Liu

Abstract: Pressure-induced structural transformations of the ammonia borane complex ($NH_3 \cdot BH_3$) were investigated in diamond anvil cells by Raman spectroscopy and synchrotron IR spectroscopy up to 14 GPa at room temperature. Starting with a disordered tetragonal structure, $NH_3 \cdot BH_3$ is found to undergo several transformations upon compression as monitored by in situ Raman measurements. These transformations are indicated by the sequential changes of characteristic Raman modes as well as by the pressure dependence of these modes. Synchrotron IR absorption spectroscopy provided supplementary and consistent information about the structural evolution of $NH_3 \cdot BH_3$ under compression. Decompression measurements on $NH_3 \cdot BH_3$ suggest the pressure-induced transformations are reversible in the entire pressure region. The combined Raman and IR data allowed analysis of possible high-pressure structures of $NH_3 \cdot BH_3$. Our study significantly complements previous high-pressure Raman studies by providing new information on the structures and stabilities of $NH_3 \cdot BH_3$.

Key words: ammonia borane, hydrogen storage, high pressure, Raman spectroscopy, IR spectroscopy, diamond anvil cell.

Résumé : Opérant à la température et à des pressions allant jusqu'à 14 GPa et faisant appel à la spectroscopie Raman et à la spectroscopie infrarouge (IR) synchrotron avec une cellule avec contre-partie de diamant, on a étudié les transformations induites par la pression du complexe ammoniac-borane ($NH_3 \cdot BH_3$). Tel qu'on a pu l'observer par des mesures Raman in situ, on a trouvé que, par compression, le $NH_3 \cdot BH_3$ subit plusieurs transformations à partir de sa structure tétragonale désordonnée initiale. Ces transformations sont caractérisées par des changements séquentiels des modes Raman caractéristiques ainsi que par l'influence de la pression sur ces modes. La spectroscopie d'absorption IR synchrotron fournit des informations supplémentaires et consistantes au sujet de l'évolution structurale du $NH_3 \cdot BH_3$ soumis à une compression. Des mesures de décompression sur le $NH_3 \cdot BH_3$ suggèrent que les transformations induites par la pression sont réversibles sur l'ensemble de la région de pression. Les données combinées des spectroscopies Raman et IR permettent de faire une analyse des structures du $NH_3 \cdot BH_3$ à haute pression. Ce travail apporte des compléments aux études antérieures par spectroscopie Raman en fournissant de nouvelles informations sur les structures et les stabilités du $NH_3 \cdot BH_3$.

Mots-clés : ammoniac-borane, emmagasinage de l'hydrogène, haute pression, spectroscopie Raman, spectroscopie infrarouge, cellule avec contre-partie de diamant.

[Traduit par la Rédaction]

Introduction

The ammonia borane complex ($NH_3 \cdot BH_3$) has received intensive investigation in recent years because of its promising potential as a hydrogen storage material.[1,2] Ammonia borane is a chemical hydride with high gravimetric (19.6 wt% H) and volumetric (145 gH L^{-1}) hydrogen density and low molecular mass (30.7 g mol^{-1}). At room temperature and ambient pressure, $NH_3 \cdot BH_3$ is a stable solid, neither flammable nor explosive. Heating $NH_3 \cdot BH_3$ releases hydrogen at temperatures from 350 to 410 K to yield polyaminoborane $(BH_2NH_2)_x$.[3–5] The reaction is moderately exothermic ($\Delta H = -21$ kJ mol^{-1}).[6] Continued heating releases a second equivalent hydrogen at temperatures from 380 to 470 K, yielding polyiminoborene $(BHNH)_x$ and trace quantities of borazine $(B_3N_3H_6)$.[6–9]

In addition to the hydrogen storage development, the molecular and electronic structures of ammonia borane are of fundamental interest. Although the ammonia borane complex is isoelectronic with gaseous ethane at ambient conditions, it contains a highly polarized dative N→B bond (μ = 5.1 D) formed by the electron donor–acceptor pair. The N→B bond has a dissociation energy of ~130 kJ mol^{-1},[10] which is much stronger than a typical van der Waals interaction. In addition, this dative bond is much shorter (1.58 Å)[11] in the molecular solid than in the gas phase (1.67 Å).[12] As a result, ammonia borane forms a stable molecular solid under ambient conditions that is characterized by strong dipole–dipole interactions in the crystalline network. More significantly, this complex is known to contain "dihydrogen" bonding. A dihydrogen bond is an unconventional hydrogen bond with, for example, N–H···H–B intermolecular interactions in $NH_3 \cdot BH_3$ crystals, with 2.02 Å being the shortest H–H distance.[11] Typically, dihydrogen bonding is characterized by a short H–H contact distance (<2.2 Å) and a strongly bent angle (i.e., the angle between N–H and H–B). The effects of dihydrogen bonding on the

Received 19 March 2009. Accepted 23 June 2009. Published on the NRC Research Press Web site at canjchem.nrc.ca on 20 August 2009.

S. Xie and Y. Song.[1] Department of Chemistry, The University of Western Ontario, London, ON N6A 5B7, Canada.
Z. Liu. Geophysical Laboratory, Carnegie Institution of Washington, DC 20015, USA.

[1]Corresponding author (e-mail: yang.song@uwo.ca).

vibrational dynamics of the molecular crystal were recently demonstrated using incoherent inelastic neutron scattering.[13] These structural characteristics, including bond strength, bond length, and the directionality of dihydrogen bonding, critically determine the molecular and crystal symmetries and, therefore, the stabilities of $NH_3{\cdot}BH_3$.

$NH_3{\cdot}BH_3$ crystal structures have been examined using X-ray diffraction techniques.[14–16] At room temperature, $NH_3{\cdot}BH_3$ adopts a tetragonal structure with the space group $I4mm$ (C_{4v}^9) and cell parameters $a = b = 5.240$ Å and $c = 5.028$ Å.[15–18] Each unit cell contains two molecules occupying 2a Wyckoff sites with a C_{3v} molecular axis that coincides with the C_{4v} site symmetry (Fig. 1*a*).[16–18] This molecular crystal undergoes a phase transition from an orientationally disordered tetragonal phase to an orthorhombic structure (Fig. 1*b*) when cooled to 225 K, resulting in a significant change in the lattice dynamics. However, the molecular structure of the $NH_3{\cdot}BH_3$ molecule is preserved.[19] This orthorhombic structure was shown to have the space group $Pmn2_1$ with two molecules per unit cell and the parameters $a = 5.517$ Å, $b = 4.742$ Å, and $c = 5.020$ Å. At this temperature the NH_3 and BH_3 groups are "frozen" such that an ordered structure with a staggered conformation is formed with coinciding N–B and c axes. The crystal structure reveals that the complex has C_s symmetry only, although a recent low-temperature ^{2}H NMR study suggests that the symmetry of the molecule is very close to C_{3v}, and, therefore, it largely retains its symmetric gas-phase structure.[20]

Furthermore, $NH_3{\cdot}BH_3$ has been studied extensively using vibrational spectroscopy under varying conditions. Early IR and Raman studies on ammonia borane and its isotopologues focused on the nature and behaviour of the B–N bond.[21–23] Subsequent studies investigated the vibrational frequencies of ammonia borane (and its isotopologues) using an argon matrix[21] and by performing computational work on free molecules.[24,25] More recently, Hess et al.[19] have used Raman spectroscopy to study single-crystal ammonia borane complexes at temperatures as low as 88 K. In addition, ammonia borane has been studied under pressures as high as 4 GPa using Raman spectroscopy[22,26] to investigate the pressure effects of dihydrogen bonds on the crystalline network. It is well known that the vibrational frequencies of molecular solids under pressure exhibit a blue shift because the corresponding chemical bonds stiffen as a result of the compression. In contrast, it has been well documented that, during compression, the stretching mode of A–H shifts to lower frequencies when A–H acts as the proton donor and forms an A–H···A hydrogen bond, which subsequently weakens the A–H bond. By analogy, an N–H···H–B dihydrogen bond is expected to form in the ammonia borane complex because of the short distance between the two hydrogens, where N–H acts as the proton donor and H–B acts as the proton acceptor. This dihydrogen bond model is confirmed by the observation of a red shift in the N–H stretch frequency and a blue shift in the B–H stretch frequency with increasing pressures.[22,26] In addition, pressure-induced phase transitions were reported in both studies, but with different transition pressures and detailed spectroscopic features.[22,26]

Although ammonia borane has been studied extensively, more questions remain about the structures and properties of ammonia borane at higher pressure regions. For example, will ammonia borane form any other structures in addition to the observed tetragonal and orthorhombic phases? Will the continuous weakening of the N–H bond when compressed result in dissociation or other chemical transformations in which hydrogen is discharged? Addressing these questions, especially the possibility of hydrogen discharge and reverse processes with pressure variations, is of fundamental interest for developing this potential hydrogen storage material. Therefore, it is critical to investigate the stability, inter- and intra-molecular interactions, transformations, and reversibility of ammonia borane subjected to greater compression. Here we report the in situ high-pressure study of $NH_3{\cdot}BH_3$ by Raman and IR spectroscopy using synchrotron light sources up to 14 GPa using the diamond anvil cell (DAC) technique.[27] We note that this complex was recently studied under pressures as high as 20 GPa using Raman spectroscopy by Lin et al.[28] In this study, two new possible phase transitions were identified at 5 and 12 GPa. Although we observed some similar ammonia borane transitions, we also observed new pressure-induced structural transformations. To our knowledge, this is the first time that IR measurements, which provide sensitive and quantitative structural information, have been performed on this complex at high pressures in situ. In addition, we obtained the first high-quality spectroscopic data in the lattice region, especially in the far-IR spectral measurements. The combined spectroscopic techniques used allowed us to perform an in-depth analysis on the high-pressure structures and stabilities of the complex. Compared with previous Raman studies, this study provides the most comprehensive understanding of the pressure behaviours and structures of $NH_3{\cdot}BH_3$.

Fig. 1. Ambient-pressure crystal structures and temperature-induced transitions of $NH_3{\cdot}BH_3$. The coordinate systems showing the orientations of the unit cell are indicated. The color codes for atoms are: boron (pink), nitrogen (blue), and hydrogen (white). (*a*) The tetragonal structure of $NH_3{\cdot}BH_3$ with space group $I4mm$ ($Z = 1$) at room temperature is shown. Because of the orientational disorder associated with the free rotation of the NH_3 and BH_3 groups, the hydrogen atoms are not shown. (*b*) The ordered orthorhombic structure of $NH_3{\cdot}BH_3$ formed at 225 K with space group $Pmn2_1$ ($Z = 2$) is shown.

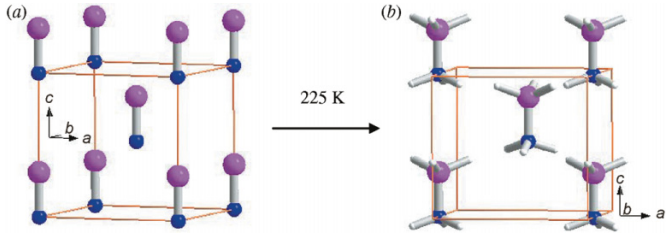

Experimental

Ammonia borane as a fine crystalline white powder with ~97% purity was purchased from Sigma-Aldrich and used without further purification. The purity was checked by ambient-pressure Raman spectroscopy and all observed Raman modes were found to be associated with the complex without any unassignable modes that originated from impurities. A symmetrical DAC with two type-I diamonds each with a 400 μm culet was used for the high-pressure Raman meas-

urements, while a pair of type II diamonds with a culet size of 300 μm was used for the IR measurements. A stainless steel gasket sample chamber was preindented to 70 μm thickness, and a 150 μm wide hole was drilled in the center. $NH_3{\cdot}BH_3$ was loaded in a MBraun LABmaster 130 glovebox equipped with a 20× microscope on the front panel. A dry inert atmosphere of <20 ppm O_2 and H_2O was maintained to accommodate the hygroscopicity of the material. The samples were loaded at room temperature with slightly elevated ambient pressures and then carefully pressurized incrementally. After each pressure change, the samples were allowed to equilibrate for a few minutes before subsequent spectroscopic measurements were taken. A few ruby (Cr^{3+} doped α-Al_2O_3) chips were used as a pressure calibrant and carefully placed inside the gasket chamber before the sample was loaded. The pressure was determined by using the R_1 ruby fluorescence line pressure shift with an accuracy of ±0.05 GPa under quasi-hydrostatic conditions.[29] For the entire pressure region, ruby fluorescence spectra obtained on different ruby chips across the sample chamber indicated no significant pressure gradient. The ruby spectral profiles suggested no obvious non-hydrostatic effects, particularly at the lower pressure regions (e.g., <10 GPa). Therefore, no pressure transmission media were used.

Raman experiments were carried out with a customized Raman microspectroscopy system constructed in our lab. A 488 nm line from an Innova Ar^+ laser (Coherent Inc.) was used as the excitation source. The laser was focused to <5 μm on the sample by an Olympus 20× objective and a 15× eyepiece and a digital camera allowed precise alignment of the focused laser beam. The Raman scattering signal was collected by the same objective lens with backscattering geometry. The Rayleigh scattering was removed by a pair of notch filters that enabled a spectral range >100 cm^{-1} to be measured before the total scattered photons were focused on the entrance slit of a spectrometer. The scattered light was then dispersed using an imaging spectrograph that housed a 0.5 m focal distance monochromator equipped with multiple gratings. A 1800 lines/mm grating with 0.1 cm^{-1} resolution was used. The Raman signal was recorded using an ultrasensitive, liquid nitrogen cooled, back-illuminated, charge-coupled device (CCD) detector from Acton. The system was calibrated using neon lines with an uncertainty of ±1 cm^{-1}. As a result of the strong diamond T_{2g} Raman mode at 1334 cm^{-1}, the spectra were collected in ranges of 50 to 1300 cm^{-1} and 1400 to 3500 cm^{-1} in several dispersive collection windows. These frequency ranges allowed all active ammonia borane Raman modes to be observed. The Raman signal was collected for 20 s for each window, and the average laser power on the sample was maintained at ~30 mW. Pressure effects on ammonia borane were examined both in the compression and decompression directions. All experiments were conducted at room temperature at pressures of up to 13.5 GPa and reproduced several times.

Infrared experiments were performed at the U2A beamline at the National Synchrotron Light Source (NSLS) at Brookhaven National Laboratory (BNL). The IR beam from the storage ring was extracted through a wedged diamond window from a source in a 40 × 40 mrad solid angle and was collimated to a 3.8 cm diameter beam before entering a Bruker IFS 66V vacuum FTIR spectrometer in conjunction with three microscope systems. The spectrometer was equipped with a number of beam splitters and detectors including a silicon bolometer and MCT. For mid-IR measurements, the IR beam was focused onto the sample by a Bruker IR microscope and then the spectrum was collected in transmission mode by the MCT detector in the 600–4000 cm^{-1} spectral range. The far-IR spectra of $NH_3{\cdot}BH_3$ were collected using a customized IR microscope with high collection efficiency and recorded by the bolometer in the 100–600 cm^{-1} spectral region. A resolution of 4 cm^{-1} was used in all IR measurements. For IR measurements, a sample thickness of 35 μm was used to allow sufficient IR transmission measurements. For all measurements, mid-IR spectra were collected through a 30 × 30 μm^2 aperture, whereas the effective IR transmission area covered the entire sample (i.e., a circle of ~90 μm in diameter) for the far-IR measurements. The reference spectrum, i.e., the diamond anvil absorption at ambient pressure, was later divided as background from each sample spectrum to obtain the absorbance. IR spectra in the decompression sequence (in ~2 GPa decrements) were also collected to investigate the reversibility of the pressure effect.

Results and discussion

Raman spectra of $NH_3{\cdot}BH_3$ during compression

Raman spectra of ammonia borane were collected from ambient pressures up to 13.5 GPa. Selected spectra are shown in Fig. 2 in four regions based on the molecular nature of the complex: the lattice region (50–600 cm^{-1}), the B–N stretching, the BH_3/NH_3 deformations and NBH rocking region (600–1650 cm^{-1}), the B–H stretching region (2100–2700 cm^{-1}), and the N–H stretching region (2750–3400 cm^{-1}).

At ambient pressure and room temperature, $NH_3{\cdot}BH_3$ crystallizes into a tetragonal phase with space group *I*4*mm* with two $NH_3{\cdot}BH_3$ molecules per unit cell.[16–18] Using factor group analysis[19], 12 distinct modes, including 11 internal modes plus one lattice librational mode, are predicted to be both Raman and IR active for the tetragonal phase of $NH_3{\cdot}BH_3$. Initially, a Raman spectrum measured at room temperature and ambient pressure is depicted at the bottom of Figs. 2*a*–2*d*. As shown, all Raman active modes except one (i.e., B–N torsion mode ν_6) are observed as predicted, in good agreement with previously reported Raman data.[19] Mode assignments are labeled in Fig. 2 and listed in Table 1. Compared with those observed in Ar-matrix isolated molecules, the N–H stretching modes (ν_7 and ν_1) in our powder sample are significantly red-shifted by 67 and 84 cm^{-1}, respectively, as a result of the dihydrogen bond in the solid phase. The analogous B–H modes (ν_8 and ν_2) are blue-shifted by 39 and 60 cm^{-1}, respectively. The assignment of the B–N stretching mode, which was originally assigned to be 787 cm^{-1} in ether solution by Taylor and Cluff[21], has long been disputed. Taylor and Cluff's assignment was confirmed by Sawodny and Goubeau[23] with a similar value of 776/790 cm^{-1} ($^{11}B/^{10}B$); however, it was reassigned by Smith et al.[30] to be 968/987 cm^{-1} ($^{11}B/^{10}B$) in argon matrices and by Jagielska et al.[31] to be 1005 cm^{-1} using an ab initio calculation.[31] In our research, we observed the B–N stretching mode (ν_5/ν_5') at 783/798 cm^{-1} ($^{11}B/^{10}B$), consistent with the original assignment and some recent observations,[22,26,28] indicating that the

Fig. 2. Selected Raman spectra of $NH_3{\cdot}BH_3$ collected at room temperature on compression in the spectral region of (*a*) 50–600 cm^{-1}, (*b*) 600–1650 cm^{-1}, (*c*) 2100–2700 cm^{-1}, and (*d*) 27503400 cm^{-1}. The relative intensities are normalized and thus are directly comparable. Because of the intense T_{2g} Raman mode of the diamond anvil at 1332 cm^{-1}, the region of 1270–1440 cm^{-1} is truncated in (*b*).The pressures in GPa are labeled for each spectrum. The assignments of Raman modes are labeled for several spectra. Unassigned peaks are labeled with asterisks (see text). The spectra are offset vertically for clarity.

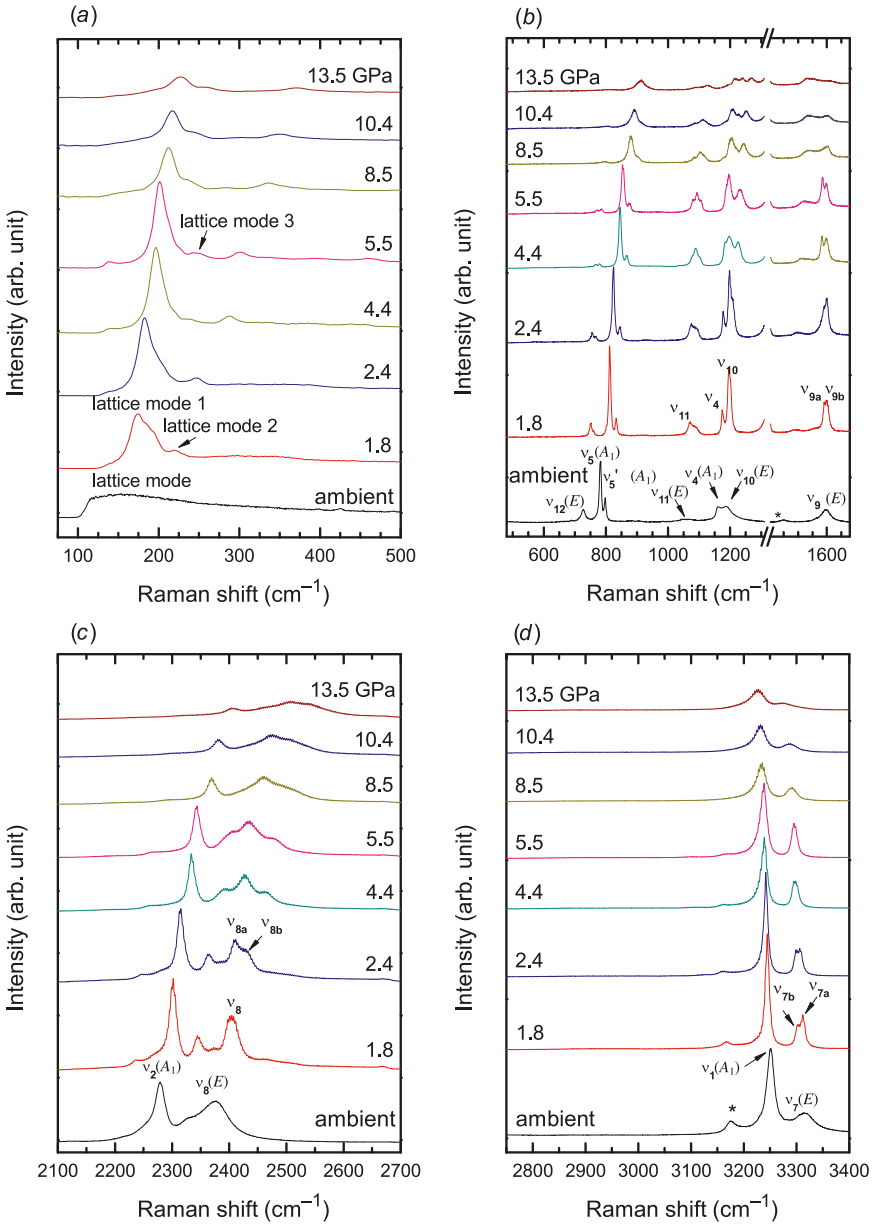

structure and behaviour of $NH_3{\cdot}BH_3$ in argon matrices is closer to the gas phase than the solid phase. For peaks at 1067 and 728 cm^{-1}, the NBH rocking modes (ν_{11} and ν_{12}) assignment of Hess et al.[19] was adopted, which are described as rocking motions involving planes of hydrogen atoms from both the NH_3 and BH_3 groups. Several previously observed but unassigned peaks, such as those at 3175 and 1447 cm^{-1}, for example, are also seen.[19,22,26] On the basis of limited polarized measurements,[19] the peak at 3175 cm^{-1} is assigned as polarized, whereas the peak at 1447 cm^{-1} is a depolarized mode.

Upon compression from ambient pressure to 1.8 GPa, a phase transition can be identified by the splitting of the modes with *E* symmetry, as well as the by the significant narrowing of the lattice mode (Fig. 2). For instance, the doubly degenerate modes ν_7 (asymmetrical N–H stretching) at 3319 cm^{-1} and ν_9 (NH_3 deformation) at 1595 cm^{-1} each split into two modes, i.e., ν_{7a}/ν_{7b} (3303 cm^{-1}/3312 cm^{-1}) and ν_{9a}/ν_{9b} (1593 cm^{-1}/1602 cm^{-1}). The phase transition is also apparent by the development of the lattice mode near 141 cm^{-1} at ambient pressure, which becomes more pronounced and finally evolves into two lattice modes at 174 and 220 cm^{-1} at 1.8 GPa. The sharp lattice modes strongly suggest a phase transition from the disordered tetragonal structure at ambient pressure to an ordered structure at 1.8 GPa. It is also noted that modes ν_4 and ν_{10}, which are

Table 1. Raman modes of ammonia borane observed under different conditions.

This work (cm^{-1})[a]	Ether solution (cm^{-1})[b]	Crystal (cm^{-1})[c]	Crystal (cm^{-1})[d]	Powder (cm^{-1})[e]	Assignment	Mode
3319	3309	3316	3316	3312	ν_7 (E)	Asym. N–H stretch
3253	3183	3250	3255	3245	ν_1 (A_1)	Sym. N–H stretch
2376	2316	2328	n.o.	2316	ν_8 (E)	Asym. B–H stretch
2280	2285	2279	2280	2277	ν_2 (A_1)	Sym. B–H stretch
1595	1600	1600	1596	1597	ν_9 (E)	NH_3 deformation
1377	n.o.	1357	1375	1374	ν_3 (A_1)	NH_3 deformation
1188	1175	1189	1185	1165	ν_{10} (E)	BH_3 deformation
1161	n.o.	1155	1158	n.o.	ν_4 (A_1)	BH_3 deformation
1067	1060	1065	1066	1058	ν_{11} (E)	NBH rock
798	n.o.	800	798	790	ν_5'(A_1)	^{10}B–N stretch
783	787	784	782	776	ν_5 (A_1)	^{11}B–N stretch
728	n.r.	727	726	715	ν_{12} (E)	NBH rock
141	n.r.	n.r.	175[f]	n.r.	Lattice mode	

Note: n.o., not observed; n.r., not reported.

[a]Measured at room temperature and ambient pressure.
[b]From ref. 21.
[c]From ref. 19.
[d]From ref. 22.
[e]From ref. 23, at low temperature.
[f]Raman shift at 1.9 GPa (see text).

very close to each other at ambient pressure, become sharply resolved at 1.8 GPa, whereas the very weak NBH rocking mode ν_{11} (1067 cm^{-1}) is greatly enhanced. In addition, a new peak appears at 2344 cm^{-1}, which was also observed but unassigned in some earlier studies.[19,22,26,28] This unassigned mode is likely a depolarized band.[19]

Upon further compression to 13.5 GPa, rich Raman features were observed to reveal the pressure-induced structural revolutions. As seen in Fig. 2*a*, the most prominent peak in the lattice in the whole pressure region is lattice mode 1, which appears at 174 cm^{-1} at 1.8 GPa. This mode becomes sharper and more intense as pressures increase to 5.5 GPa, at which point it noticeably broadens with decreasing intensity when compressed to 13.5 GPa. Lattice mode 2, although very weak at 1.8 GPa, is a characteristic mode of the new phase that is different than the disordered tetragonal structure and remains distinct as pressures increase to 13.5 GPa. The most prominent change in the lattice region is the observation of a third lattice mode at 245 cm^{-1} at 5.5 GPa, indicating a possible transformation of the crystal structure of $NH_3{\cdot}BH_3$. In addition, a clearly developed mode at 140 cm^{-1} was also observed at this pressure. These new modes, together with lattice mode 2, become weaker with increasing pressure such that only lattice mode 1 remains the dominant mode at 13.5 GPa. We note that in previous Raman studies only two lattice modes were observed in all pressure regions,[28] which is in strong contrast to our results. It is likely that the missing mode at 140 cm^{-1} is associated with the detection limit achieved.

The internal modes in the spectral region 600–1650 cm^{-1} (Fig. 2*b*), including the ν_{12}, ν_{11}, ν_{10}, and ν_9 modes when compressed to 2.4 GPa, are characterized by further splitting of the doubly degenerate modes with E symmetry during compression. Upon further compression to 5.5 GPa, these modes exhibit the maximum splitting with the exception of ν_7, which merged into a singlet. Continuous compression from 5.5 to 8.5 GPa results in merging with a markedly reduced intensity for most of the modes. All modes are significantly broadened when compressed above 13.5 GPa. These observations are in general agreement with those of Lin et al.,[28] except for the detailed profile of a few bands. For instance, the NH_3 deformation mode (ν_9) at ~1600 cm^{-1} that exhibits clear splitting up to 5.5 GPa shows a drastically different profile: no splitting was observed in the entire pressure region.[28]

The splitting at ν_5 mode is due to an isotopic effect rather than the removal of degeneracy. The ^{11}B and ^{10}B contributions to the B–N symmetric stretch (ν_5 and ν_5') are readily apparent up to 8.5 GPa. Both ^{11}B–N (ν_5) and ^{10}B–N (ν_5') stretching modes are sharp in the pressure region under 5.5 GPa, whereas ν_5' is much weaker than ν_5 because of the lower abundance of ^{10}B (19.9%). The frequency difference at 8.5 GPa is ~19–21 cm^{-1}, which is larger than that observed under ambient conditions (i.e., 15 cm^{-1}). However, this value is still in agreement with the frequency difference of 18 cm^{-1} reported by Custelcean and Dreger[22] and of 20 cm^{-1} observed by Lin et al.[28]

The symmetric B–H stretching mode ν_2 (A_1), one of the most intense Raman bands at ambient pressure, exhibits a pressure-induced blue shift and weakening (Fig. 2*c*); it becomes significantly broadened above 8.5 GPa. The doubly degenerate asymmetric B–H stretching mode ν_8 readily splits when compressed to 2.4 GPa, exhibiting a strongly asymmetric doublet labeled as ν_{8a} and ν_{8b}. As pressures continue to increase, mode ν_{8a} becomes most pronounced at 4.4 GPa and subsequently becomes much broader at higher pressures (e.g, 8.5 GPa) because of coalescence with ν_{8b} and a nearby depolarized peak.[19] In contrast to the BH stretching modes, both the symmetric and asymmetric N–H stretching modes shift to red with increasing pressures (Fig. 2*d*). The symmetric N–H stretching mode ν_1 with A_1 symmetry, the most intense $NH_3{\cdot}BH_3$ Raman band in the en-

Fig. 3. Pressure dependences of the Raman shift of $NH_3{\cdot}BH_3$ on compression for (*a*) the lattice modes, (*b*) the BH_3 deformation (ν_{10a}, ν_{10b}, and ν_4) and NH_3 deformation (ν_{9a} and ν_{9b}) modes, (*c*) the $^{11}B–N/^{10}B–N$ stretch (ν_5/ν_5') modes, (*d*) the NBH rock (ν_{12a}, ν_{12b}, ν_{11a}, ν_{11b}, and ν_{11c}) modes, and (*e*) the N–H stretch (ν_{7a}, ν_{7b}, and ν_1) and B–H stretch (ν_{8a}, ν_{8b}, and ν_2) modes. Different symbols denote Raman modes with different origins. The solid lines crossing the solid symbols are based on linear fit. The vertical dashed lines indicate the proposed phase boundaries.

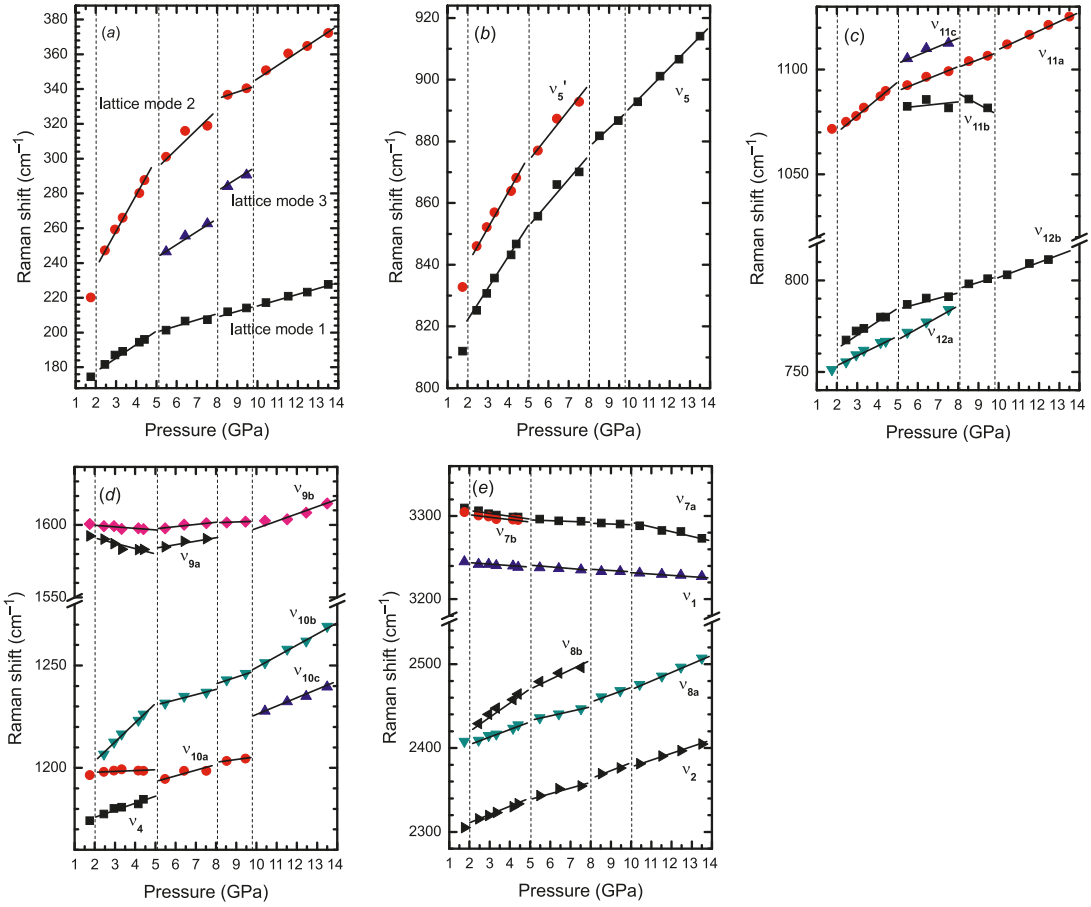

tire pressure region, becomes much broader and weaker when compressed to 8.5 GPa. The asymmetric N–H stretching mode ν_7 (*E*) that displays a doublet (ν_{7a} and ν_{7b}) at 1.8 GPa becomes a convoluted mode on compression. Similar to the ν_1 mode, this mode also broadens markedly beyond 8.5 GPa. Above 13.5 GPa, this mode is barely visible. These observations are consistent with those of Lin et al.[28]

Pressure effects on Raman modes of $NH_3{\cdot}BH_3$

To confirm the possible phase transformations on compression, the pressure dependence (i.e., Raman shift versus pressure) of selected Raman modes are depicted in Fig. 3. Calculated pressure coefficients ($d\nu/dP$ (cm^{-1} GPa^{-1})) for the monitored peaks obtained by linear regression of the experimental data are listed in Table 2. Phase transitions are further indicated when sharp differences in pressure coefficients are observed. Compared with previous analysis,[28] more phase boundaries were identified in this study.

In general, most Raman modes exhibit pressure-induced blue shifts, consistent with the finding that the bonds stiffen upon compression. However, both the symmetric and asymmetric N–H stretching modes (ν_7 and ν_1) undergo red shifts with increasing pressures in all pressure regions (i.e., $d\nu/dP < 0$), indicating the weakening of the N–H bond. This is believed to be a result of the lengthening of the N–H bond owing to the formation and strengthening of the dihydrogen bonding (N–H···H–B) as pressures increase. In strong contrast, the stretching modes (ν_8 and ν_2) involving the B–H proton acceptor group in the dihydrogen bond exhibit large blue shifts with pressure. For example, $d\nu_8/dP$ has the largest pressure coefficients (16.1 and 10.3 cm^{-1} GPa^{-1} in the 2.4–5.5 and >10.4 GPa pressure regions, respectively) indicating the significant strengthening of B–H bonding with decreasing bond length. Because the N–H and B–H bond strengths become strongly disproportionate when compressed, and the B–N bond is strengthened ($d\nu_5/dP > 0$), it is reasonable to speculate that at certain high pressures, the N–H bond may break and new materials may form.

As shown in Fig. 3 and Table 2, the pressure dependences of the major Raman modes collectively indicate several distinct pressure regions at which $NH_3{\cdot}BH_3$ could exist as different phases. These pressure regions are 2.4–5.5, 5.5–8.5, 8.5–10.4, and >10.4 GPa, which we label as phases III, IV, V, and VI, respectively (phases I and II are the known room-temperature tetragonal phase and low-temperature orthorhombic phase, respectively). In general, the pressure coefficients of the stretching modes are noticeably larger for phase III than for phase IV, which are larger than those for

Table 2. Pressure dependence of the Raman modes of $NH_3{\cdot}BH_3$ on compression.

			$d\nu/dP$ (cm^{-1} GPa^{-1})			
Mode	Assignment	Raman shift (cm^{-1})[a]	Phase III (2.4–5.5 GPa)	Phase IV (5.5–8.5 GPa)	Phase V (8.5–10.4 GPa)	Phase VI (>10.4 GPa)
Lattice mode 1		141	6.3	2.9	2.4	3.3
Lattice mode 2			17.8	8.6	4.0	6.7
Lattice mode 3				7.8	7.1	8.2
Asym. N–H stretch	ν_{7a}	3319	–3.1/–2.7[b]	–1.2	–1.6	–4.6
Sym. N–H stretch	ν_1	3253	–1.5	–0.9	–1.1	–1.3
Asym. B–H stretch	ν_8	2376	8.7/16.1[c]	5.3/8.3[c]	7.8	10.3
Sym. B–H stretch	ν_2	2280	9.2	5.6	7.4	7.6
^{11}B–N stretch	ν_5	783	5.2	3.7	5.3	6.8
^{10}B–N stretch	ν_5'	798	6.2	5.0		
NBH rock	ν_{11a}	1067	6.1	3.3	2.8	4.4
	ν_{11b}			0.6/3.6[d]	0.2	
	ν_{12}	728	5.2/6.2[e]	6.1/2.0[e]	3.0	4.1
NH_3 deformation	ν_9	1595	–2.3/–0.6[f]	2.7/1.7[f]	0.5	3.9
	ν_3	1377	–0.3	–0.8		
BH_3 deformation	ν_{10a}	1067	0.3	1.9	1.2	
	ν_{10b}		8.3	2.6	1.3	5.6/3.7[g]
	ν_4	1161	3.1			

[a]Measured at ambient pressure and room temperature.
[b]ν_{7a}/ν_{7b}.
[c]ν_{8a}/ν_{8b}.
[d]ν_{11b}/ν_{11c}.
[e]ν_{12a}/ν_{12b}.
[f]ν_{9a}/ν_{9b}.
[g]ν_{10b}/ν_{10c}.

phase V. The pressure coefficients of the rocking and deformation modes, however, do not exhibit consistent trends along phase transformations. Interestingly, the pressure coefficients of these modes seem to become larger again when compressed beyond 10.4 GPa. In summary, although the phase boundaries of 2.4 and 5.5 GPa observed in this study can be roughly aligned with those at 2 and 5 GPa noted previously,[28] new phase boundaries along with more high-pressure phases are observed in the present study.

Raman spectra of $NH_3{\cdot}BH_3$ during decompression

The reversibility of pressure effects on molecular structures provides important information on transformation mechanisms. Therefore, upon compression of $NH_3{\cdot}BH_3$ to the highest pressure of 13.7 GPa, we conducted Raman measurements on decompression all the way down to a near ambient pressure. Selected spectra are depicted in Fig. 4. In general, the change in the Raman profile is very gradual on decompression. At 13.7 GPa, one lattice mode and ν_5, ν_4, ν_{10}, ν_9, ν_8, ν_1, and ν_7 modes resolve. Starting at 6.2 GPa, the ν_2 mode at 2362 cm^{-1} recovers from decompression. Simultaneously, the ν_1 and ν_7 modes are completely deconvoluted. Further decompression to 4.0 GPa results in the development of ν_5', ν_{511}, and $\nu_{9a,b}$ modes. The onset pressure for the observation of ν_{12} and ν_4 along decompression is 2.3 GPa. When the pressure is reduced to 0.8 GPa, the Raman profile is almost identical to that at 1.8 GPa on compression. These observations suggest that, although there is some hysteresis upon decompression characterized by "delayed" back-transformations, the pressure-induced phase transitions are reversible in the entire pressure range in this study.

Mid-IR spectra of $NH_3{\cdot}BH_3$

Figure 5*a* shows the mid-IR absorption spectrum of $NH_3{\cdot}BH_3$ measured at room temperature and at 1.5 GPa (the first pressure point on compression). According to a factor group analysis,[19] all spectral active modes of $NH_3{\cdot}BH_3$ are both IR and Raman active. Therefore, the fundamental IR modes can be assigned by comparing our IR spectrum with previous IR and Raman measurements as reported in Table 3. In addition, vibrational frequencies observed from low-temperature inelastic neutron scattering (INS) measurements, which have no selection rules, are also listed to confirm the assignments in the spectra region below 1400 cm^{-1}.[25] In contrast to the Raman spectra, many more IR bands are observed as a result of overtones and (or) combinations of fundamental modes, which are labeled with asterisks in Fig. 5*a*. For instance, a new band is observed at 3479 cm^{-1}, which is very close to the combination of ν_{11} and ν_3 as $2\nu_{11} + \nu_3$, where ν_{11} = 1055 cm^{-1} and ν_3 = 1362 cm^{-1}. Similarly, the bands at 2674, 2123, and 1483 cm^{-1} are likely to be overtones of ν_3 (1362 cm^{-1}), ν_{11} (1055 cm^{-1}), and ν_{12} (751 cm^{-1}) as $2\nu_3$, $2\nu_{11}$, and $2\nu_{12}$, respectively. The band at 1767 cm^{-1} is not coincident with any combination of internal modes, but it is likely a combination of lattice modes and internal modes. Although some modes could not be distinguished because of the saturated absorptions in regions 1050–1250 cm^{-1} and 3150–3400 cm^{-1}, all

Fig. 4. Selected Raman spectra of $NH_3{\cdot}BH_3$ on decompression from 13.7 GPa all the way down to ambient pressure. The relative intensities are normalized and thus are directly comparable. The pressures in GPa are labeled for each spectrum. The spectra are offset vertically for clarity.

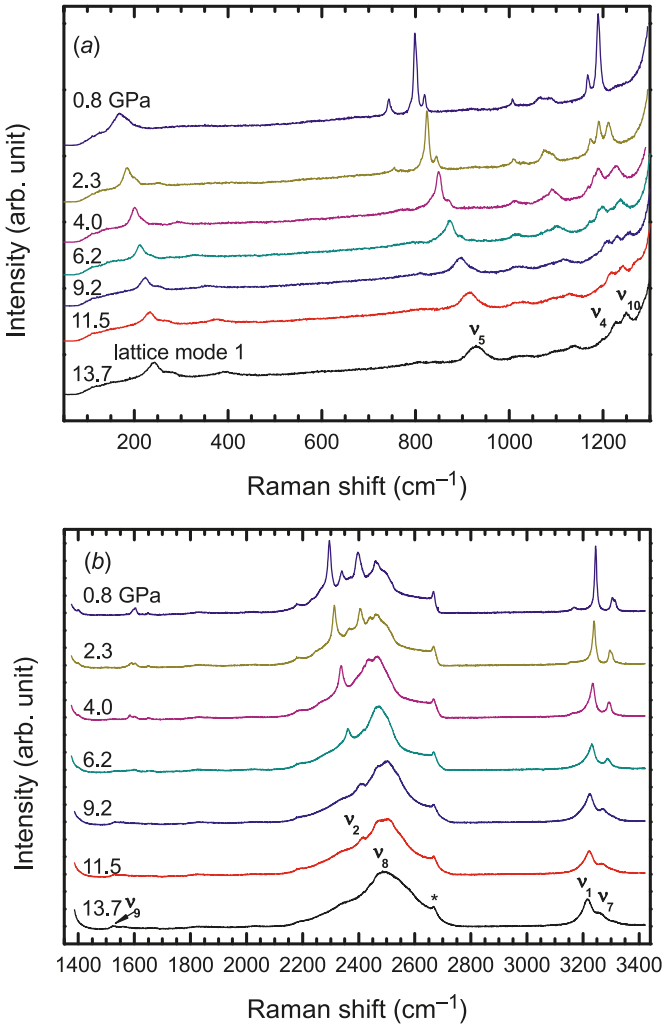

fundamental internal modes except a BH_3 deformation mode and an N–H stretching mode were observed, which is in agreement with previous Raman and IR data.[21–23]

Figure 6*a* shows the IR absorption spectra of $NH_3{\cdot}BH_3$ when compressed to 13.7 GPa at room temperature. Compared with Raman measurements on compression, the pressure evolution of the $NH_3{\cdot}BH_3$ bands is very gradual and lacks distinctive profile changes, which is mainly associated with the extremely strong or even saturated absorptions in most of the spectral regions. In addition, the absorption is markedly enhanced as pressures increase such that the multiple bands in the spectral region of 1000–1600 cm^{-1} convolute to two broad bands at 13.7 GPa. As a result, it is difficult to visualize phase transitions from the IR spectra. The only discernable profile change occurs at 7.8 GPa as indicated by the broadening of the ν_{12} mode and by the enhanced intensity of the ν_8 mode. However, the pressure dependences of the IR bands shown in Fig. 7 and Table 4 show roughly consistent pressure-induced phase transitions

Fig. 5. Synchrotron mid-IR absorption spectrum of $NH_3{\cdot}BH_3$ collected at room temperature and (*a*) 1.5 GPa upon compression in comparison with (*b*) 0.3 GPa upon decompression in the spectral region 600–3800 cm^{-1}. The assignments of the fundamental modes are shown above the corresponding IR bands. The IR bands labeled with asterisks are overtones or combinations of lattice modes and (or) internal modes (see text).

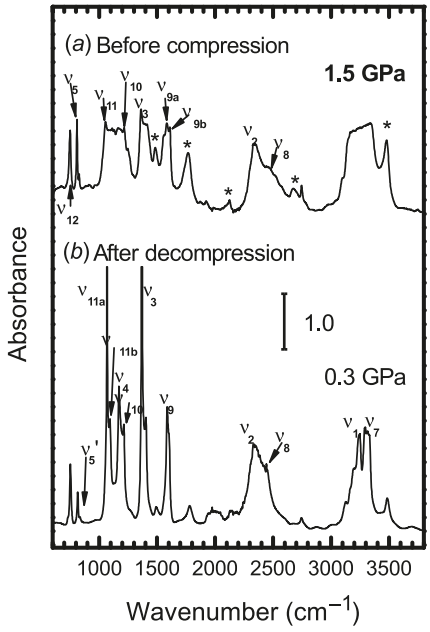

as established by our Raman measurements. Generally, most of the IR modes exhibit blue shifts with increasing pressure, consistent with the pressure-induced bond stiffening. For example, a pressure coefficient as large as 26.8 cm^{-1} GPa^{-1} is observed for the B–H stretching mode ν_8 in the pressure region of 7.8–10.8 GPa. Although the N–H stretching modes cannot be monitored owing to strong absorption, the NH_3 deformation modes (ν_{9a}, ν_{9b}, and ν_3) exhibit unambiguous red shifts, yielding consistent information obtained by Raman measurements interpreted as the weakening of N–H bonds with the formation of dihydrogen bonds.

After compressing $NH_3{\cdot}BH_3$ to pressures as high as 13.7 GPa, we conducted IR measurements on decompression to near ambient pressures (e.g., 0.3 GPa). Selected spectra are depicted in Fig. 6*b* and compared with the compression data in Fig. 6*a*. Apparently, the decompression data provide more information because the absorption is markedly reduced as the sample thins out after the compression–decompression cycle. For instance, when the pressure is reduced to 8.9 GPa, the previously saturated ν_4 and ν_{11} bands are resolved. Furthermore, IR bands ν_1 and ν_7 are clearly visible when decompressed to 2.9 GPa. Finally, as seen in Fig. 5*b*, all modes observed before compression at 1.5 GPa are recovered after decompression at 0.3 GPa. These observations indicate that the structural transformations upon compression are completely reversible in the entire pressure region, consistent with our Raman measurements.

Far-IR spectra of $NH_3{\cdot}BH_3$

Using the unique synchrotron far-IR setup dedicated to in situ high-pressure measurements, we obtained the first far-IR

Table 3. Assignment of IR fundamental frequencies for $NH_3{\cdot}BH_3$ in comparison with Raman data.

IR (cm^{-1})		INS (cm^{-1})	Raman (cm^{-1})		Assignment	IR bands
This work[a]	Reference 30[b]	Reference 25[c]	This work[d]	Reference 19[e]		
	3386		3303/3312[f]	3316	ν_7 (E)	Asym. N–H stretch
	3337		3244	3250	ν_1 (A_1)	Sym. N–H stretch
2453	2415		2404	2328	ν_8 (E)	Asym. B–H stretch
2337	2340		2302	2279	ν_2 (A_1)	Sym. B–H stretch
1584/1610[g]	1608		1593/1602[g]	1600	ν_9 (E)	NH_3 deformation
1362	1343	1368	1371	1357	ν_3 (A_1)	NH_3 deformation
1216	1186	1189	1198	1189	ν_{10} (E)	BH_3 deformation
	1175	1177	1174	1155	ν_4 (A_1)	BH_3 deformation
1055	1052	1080	1070	1065	ν_{11} (E)	NBH rock
828	987		832	800	ν_5 (A_1)	^{10}B–N stretch
810	968	798	812	784	ν_5'	^{11}B–N stretch
751	603	737	751	727	ν_{12} (E)	NBH rock

Note: INS, inelastic neutron scattering.

[a]Measured at room temperature and 1.5 GPa.

[b]At low temperature.

[c]Using inelastic neutron scattering at 30 K.

[d]Measured at room temperature and 1.8 GPa.

[e]At room temperature.

[f]Frequencies for ν_{7a}/ν_{7b}.

[g]Frequencies for ν_{9a}/ν_{9b}.

$NH_3{\cdot}BH_3$ absorption spectra at 13.5 GPa. Similar to the mid-IR region, the lattice modes in the far-IR region at 100–600 cm^{-1} are overwhelmed by extremely strong absorptions that do not allow individual modes to be identified. Therefore, we performed a compression to 13.5 GPa stepwise (the IR spectra are not shown on compression) and then measured the IR absorption on decompression with selected spectra, shown in Fig. 8*a*. At the highest pressure, two lattice modes at 294 cm^{-1} (band 1) and 415 cm^{-1} (band 2) are clearly observed. Compared with the Raman lattice region (Figs. 2*a* and 3*a*), band 1 is close to the Raman lattice mode 3 by extrapolation, whereas band 2 is a new lattice mode (IR active only). On decompression, both modes shift to lower frequencies. When decompressed to 3.5 GPa, band 1 displays enhanced absorption but subsequently diminishes into a shoulder peak when decompressed to 1.2 GPa. At this pressure, only one major band with a frequency of 210 cm^{-1} is observed, which is comparable with the Raman lattice mode 2 (219 cm^{-1}) at 1.8 GPa, but with strongly contrasting intensities.

We plotted the frequencies of the IR active modes observed in the lattice region as a function of pressure on both compression and decompression (Fig. 8*b*). Again, owing to strong absorption, $NH_3{\cdot}BH_3$ produces a broad, saturated band below 3.3 GPa upon compression. At this pressure, a clearly defined band evolved at 420 cm^{-1} (as band 3 in Fig. 8*b*) and rapidly shifted to higher frequencies ($d\nu/dP$ = 18.8 cm^{-1} GPa^{-1}) as pressures increased to 9.5 GPa when the intensity diminished almost completely. Interestingly, this band is not observed in this pressure region upon decompression, but only displays barely visible intensities below 3.5 GPa. As seen in Fig. 8, bands 1 and 2 could not be distinguished from the saturated bands until the sample was compressed to 8.5 GPa, at which point they remain resolved up to the highest pressure. Upon decompression, however, these two modes exhibit different pressure dependences (i.e., smaller pressure coefficients) than when compressed, indicating that back transformation is more sluggish owing to hysteresis. The pressure dependences of both these modes show a distinct change around 5.5 GPa, coinciding with one of the transition pressures established by our Raman measurements.

Discussion

In previous Raman studies of $NH_3{\cdot}BH_3$ in the low pressure range (i.e., <4 GPa),[22,26] two solid-to-solid transitions at 0.5 and 1.4 GPa were found by Trudel and Gilson,[26] which is different from Custelcean and Dreger's study[22] in which only one phase transition was found (at 0.8 GPa). This discrepancy may result from the differences in the hydrostatic conditions used in the two studies. Both of our Raman and IR measurements are in general agreement with these two studies in terms of phase regions, i.e., the spectroscopic features observed below and above 2 GPa roughly align with those before and after the phase transitions observed below 1.5 GPa in both studies, except that we extend the previously observed second high-pressure phase from 4 to ~5.8 GPa (we label this as phase III), which is in qualitative agreement with Lin et al.'s study.[28] Above this pressure, our Raman and IR measurements show two more phase transitions at 8.5 and 10.4 GPa, whereas the only transition observed in Lin et al.'s study was near 12 GPa.[28] In addition to the different boundaries, differences in Raman profiles, such as those in the lattice region, were also observed. One possible explanation is that our materials had a different purity and crystallinity: we used a reagent grade with a purity of 97% (purchased directly from Sigma-Aldrich), whereas Lin et al.[28] used synthetic laboratory and heat-treated samples with an unknown purity. In addition, as discussed in the following, the phase transitions are characterized by

Fig. 6. Synchrotron mid-IR spectra of $NH_3{\cdot}BH_3$ in the spectral range of 600–3800 cm^{-1} measured at room temperature for selected pressures (indicated in GPa above each spectrum) on (*a*) compression and (*b*) decompression. The absorbance has been normalized with respect to the beam current of the synchrotron light source. The spectra are offset vertically for clarity.

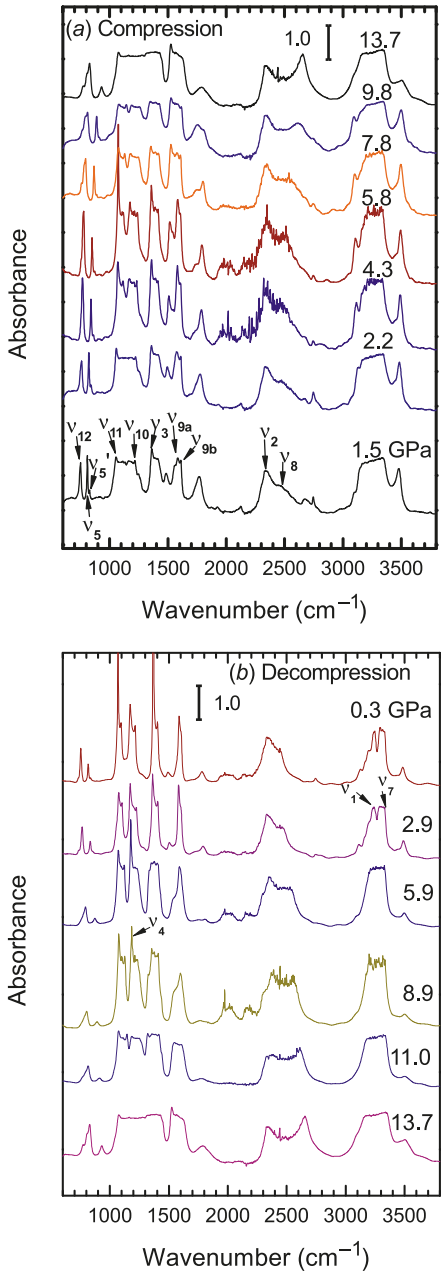

subtle changes in the unit cell without major, irreversible modifications. Such transitions are generally sensitive to compression conditions and therefore may be affected by additional factors such as kinetics. Nevertheless, our parallel measurements yielded reproducible and consistent results.

Then the remaining question is what are the possible structures of high-pressure phases of ammonia borane induced by compression and decompression. To our knowledge, no in situ high-pressure X-ray diffraction study of this complex has been reported. Therefore, these combined Raman and IR

Fig. 7. Pressure dependences of IR frequencies of $NH_3{\cdot}BH_3$ for internal modes on compression. Different symbols denote different IR origins with assignments labeled on the right-hand side. The vertical dashed lines indicate one of the proposed phase boundaries.

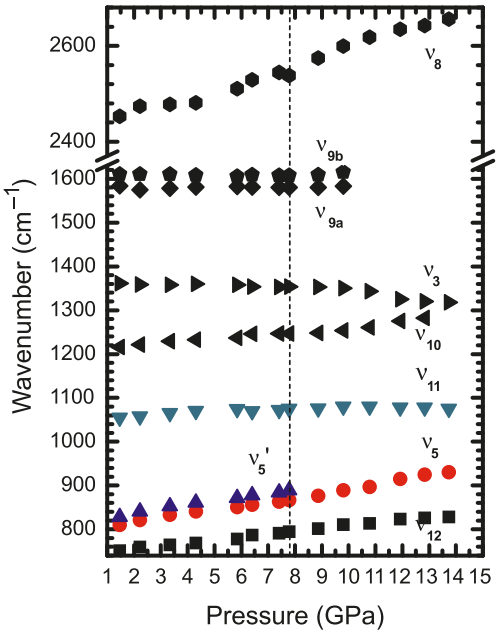

spectroscopic measurements, especially in the lattice region, provide important insight for understanding the high-pressure structures of the ammonia borane complex. Unfortunately, Hess et al.'s[19] recent low-temperature Raman study does not include lattice data, and lattice features were not analyzed in depth in any of the previous high-pressure Raman studies because of measurement limitations.[22,26]

For the phase below 2.4 GPa, the Raman measurement at 1.8 GPa (Fig. 2*a*) and IR measurement at 1.2 GPa (Fig. 8*a*) in the present study clearly indicate that there are at least two lattice modes associated with this phase. It is known that high pressures and low temperatures often induce similar phase transitions for many materials that have normal *P–T* phase diagrams. Therefore, to assume that the low-pressure phase has the same or similar crystal structure as the low-temperature orthorhombic phase is reasonable and can be examined for consistency by the observed spectroscopic features. Using factor group analysis, the orthorhombic structure ($Pmn2_1$) with two molecular units per unit cell has the following lattice modes[19]:

$$[1]\quad \Gamma^{NH_3\cdot BH_3}_{\text{lattice vib.}} = A_1 + A_2 + B_2$$
$$\Gamma^{NH_3\cdot BH_3}_{\text{lattice lib.}} = A_1 + 2A_2 + 2B_1 + B_2$$

where Γ_{vib} and Γ_{lib} are the irreducible representations for lattice vibration (translation) and lattice liberation (rotation), respectively. Species A_2 is Raman active and A_1, B_1, and B_2 are both IR and Raman active. Thus, nine lattice modes are predicted with all Raman active modes and six are IR active. Apparently, the two lattice modes observed are only a subset of the predicted modes if the assumed crystal structure is correct. Because the notch filters used in our Raman system and far-IR setup at the synchrotron beamline do not

Table 4. Pressure coefficients of the observed IR bands of $NH_3{\cdot}BH_3$ on compression.

		$d\nu/dP$ (cm^{-1} GPa^{-1})			
IR bands	Assignment	Phase III (2.8–5.8 GPa)	Phase IV (5.8–7. 8 GPa)	Phase V (7. 8–10.8 GPa)	Phase VI (>10.8 GPa)
Asym. B–H stretch	ν_8	12.6	14.6	26.8	12.4
^{11}B–N stretch	ν_5	7.6	8.1	10.6	8.5
^{10}B–N stretch	ν_5'	8.3			
NBH rock	ν_{11}	4.0	0.9	2.0	–1.6
	ν_{12}	5.1	5.5	6.5	2.6
NH_3 deformation	ν_{9a}/ν_{9b}	0.8/–2.2	–0.8/–1.4	1.4/3.8	
	ν_3	–0.1	0.0	–5.0	–3.8
BH_3 deformation	ν_{10}	2.9	0.6	6.6	8.0

allow unambiguous measurements below 100 cm^{-1}, it is possible that some additional lower frequency lattice modes were not detected. Nevertheless, the additional splitting features observed in the internal mode region, such as those for the ν_{11}, ν_9, and ν_7 modes, strongly suggest the structure is orthorhombic rather than tetragonal.

The next high-pressure phase (phase III, 2.4–5.5 GPa) may have a structure very similar to the low-pressure orthorhombic phase. This is indicated by the similarity of the lattice profile both in the Raman and IR measurements as well as in the more prominent splittings observed for the ν_{12}, ν_{11}, ν_8, and ν_9 modes. These observations strongly suggest enhanced intermolecular interactions as a result of compression as manifested by the largest pressure coefficient (Table 2) observed among all pressure regions. In addition, the bending deformation modes for BH_3 and NH_3 (i.e., ν_{10} and ν_9, respectively) at 2.4 GPa have a broad profile, indicating some degree of rotational disorder for NH_3–BH_3 along its molecular axis at this pressure. Upon compression, both modes split into narrower doublet peaks that suggests that the free rotation of the BH_3 and NH_3 groups is likely hindered by pressure and thus the complex may undergo a rotational disorder–order process in this pressure region. We note that our observation is in contrast to that of Lin et al.[28] where the splitting of these modes is lacking in this pressure region.

From 5.5 to 8.5 GPa, the complex undergoes a more prominent structural modification. In this region, up to four Raman lattice modes and three IR lattice modes were observed. The Raman frequencies are 139, 201, 246, and 301 cm^{-1} at 5.5 GPa, whereas the IR frequencies observed at the same pressure are 241, 344, and 467 cm^{-1}. However, the IR bands at 241 and 344 cm^{-1} measured during decompression are known to exhibit higher frequencies than those measured on compression owing to hysteresis. Therefore, we linearly extrapolated the high-pressure frequencies of IR bands 1 and 2 (Fig. 8*b*) to 5.5 GPa to obtain the corrected "compression" data (215 and 311cm^{-1}). As a result, these two major IR bands are roughly aligned with the two major Raman bands at 201 and 301 cm^{-1} as observed in other pressure regions, suggesting the new modes are 139 and 246 cm^{-1} for Raman measurements and 467 cm^{-1} for IR measurements. Again, because the observed Raman and IR modes are generally a subset of the predicted ones, it is difficult to perform a full factor group analysis without crystal structures. However, these observations can temporarily rule out a significant change to the factor group of the $NH_3{\cdot}BH_3$ crystal lattice, especially changes to centrosymmetric groups such as D_{2h} for orthorhombic or C_{2h} for monoclinic systems. The observation of new lattice modes can be interpreted as enhanced correlation field interactions within the C_{2v} factor group or even lower symmetry groups, such as those for monoclinic systems. X-ray diffraction measurements are required to understand the detailed structures of this $NH_3{\cdot}BH_3$ phase.

Above 8.5 GPa, both the Raman and IR spectra are characterized by significant profile broadening in almost all spectral regions. Split Raman modes are merged into broad bands with significantly reduced intensity (e.g., ν_{11}, ν_9, and ν_8), whereas the lattice modes measured both by Raman and IR spectroscopy become much weaker and broad. Above 10.4 GPa, the number of lattice modes in both Raman and IR measurements is reduced, whereas the remaining modes undergo continuing weakening and broadening. These observations suggest that the $NH_3{\cdot}BH_3$ complex is transforming from an ordered crystalline structure to a possibly disordered or ultimately amorphous structure when compressed to high enough pressures. The phase between 8.5 and 10.4 GPa can be considered as an intermediate phase for the disordering process, whereas the phase above 10.4 GPa is characterized by significant disordering. Although pressure gradients at high pressure may contribute to the profile broadening, our ruby fluorescence measurements across the sample suggest that the non-hydrostatic effect contributes only very insignificantly to this broadening.

In Lin et al.'s[28] analysis of the possible high-pressure structures based on the features of a few characteristic internal modes and the observation of two lattice modes, it is proposed that the crystal structure is unaltered in the entire pressure region. However, the additional lattice modes observed by our Raman and IR measurements clearly indicate that there is a possible pressure-induced formation of new crystal structures. They further speculate that the dimerization of ammonia borane complex may be associated with one of the high pressure phases. Again, if dimerization occurs, more internal modes with different vibrational frequencies are expected. In addition, dimerization implies that the number of the molecular unit Z halves per unit cell, which is contradictory to the observation that there was an increase in the number of lattice mode. In situ X-ray diffraction measurements are required to resolve the discrepancy between the structural interpretation of the two spectroscopic studies.

Fig. 8. (*a*) Synchrotron far-IR spectra of $NH_3{\cdot}BH_3$ in the spectral range of 100 to 700 cm^{-1} measured at room temperature for selective pressures (indicated in GPa above each spectrum) on decompression. The absorbance has been normalized with respect to the beam current of the synchrotron light source. The spectra are offset vertically for clarity. (*b*) Pressure dependences of IR frequencies of $NH_3{\cdot}BH_3$ for lattice modes. The solid symbols denote frequencies observed on compression and open symbols denote frequencies for decompression. The vertical dashed lines indicate one of the proposed phase boundaries.

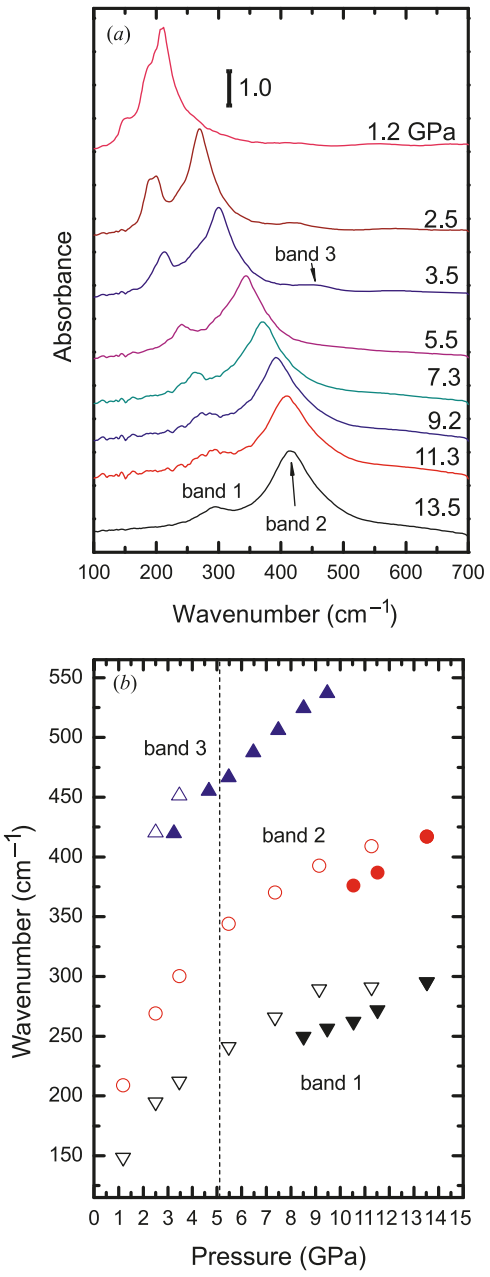

Finally, it is clear that both the Raman and IR measurements show that the pressure-induced transformations of the $NH_3{\cdot}BH_3$ complex are reversible upon decompression. The almost identical spectroscopic details in both Raman and IR internal mode regions before and after compression indicate that the chemical structure of the complex is completely unaltered by pressure and thus $NH_3{\cdot}BH_3$ is stable (i.e., no hydrogen release) up to the highest pressure yielded in this study. However, the different profiles of the lattice modes from both Raman and IR measurements suggest that crystalline structures may have been modified by pressure, even if very slightly. In addition, hysteresis has been observed in most of the pressure regions upon decompression. Our observations agree with those of Custelcean and Dreger,[22] who also found all pressure-induced transformations were reversible at <4 GPa, but that there was some hysteresis. Hysteresis is typically considered to be a result of kinetics-mediated transformations characterized by some barriers. To overcome the kinetic barrier, it would be interesting to investigate the pressure-induced transformations at elevated temperatures.

Conclusions

Using Raman and synchrotron IR spectroscopy, we investigated the pressure behaviour of the ammonia borane complex as a promising hydrogen storage material. In the low pressure region (<2 GPa), we discovered that the complex undergoes a structural transformation from a disordered tetragonal to an ordered, possibly orthorhombic, structure, consistent with previous Raman studies. Upon further compression, our Raman and IR measurements identified several solid-to-solid transformations with phase boundaries that roughly occurred at 2.4, 5.5, 8.5, and 10.4 GPa. These transformations are characterized by distinctive profiles and the pressure dependences of characteristic modes. Spectroscopic measurements on decompression suggest that these pressure-induced transformations are reversible within the intact chemical structure of the $NH_3{\cdot}BH_3$ complex, with possible modifications to the crystal structures. Analysis of combined Raman and IR measurements, especially the lattice features, suggests that $NH_3{\cdot}BH_3$ structures below 5.5 GPa resemble a low-pressure orthorhombic structure, whereas in the higher pressure regions, $NH_3{\cdot}BH_3$ complexes may undergo transformations to disordered or amorphous structures. Detailed high-pressure structural information needs to be confirmed by in situ X-ray diffraction measurements.

Acknowledgements

Y.S. acknowledges support from a Discovery Grant and a Research Tools and Instruments Grant from the Natural Sciences and Engineering Research Council of Canada (NSERC), the Leaders Opportunity Fund from the Canadian Foundation for Innovation (CFI), and the Early Researcher Award from the Ontario Ministry of Research and Innovation. IR measurements were performed at the U2A beamline at the NSLS at BNL. The U2A beamline is supported by COMPRES, the Consortium for Materials Properties Research in Earth Sciences under NSF Cooperative Agreement EAR06-49658, US Department of Energy (DOE), (CDAC), and NSF (DMR).

References

(1) Xiong, Z. T.; Yong, C. K.; Wu, G. T.; Chen, P.; Shaw, W.; Karkamkar, A.; Autrey, T.; Jones, M. O.; Johnson, S. R.; Edwards, P. P.; David, W. I. F. *Nat. Mater.* **2007**, *7* (2), 138–141. doi:10.1038/nmat2081. PMID:18157135.

(2) Dixon, D. A.; Gutowski, M. *J. Phys. Chem. A* **2005**, *109* (23), 5129–5135. doi:10.1021/jp0445627. PMID:16833867.
(3) Stowe, A. C.; Shaw, W. J.; Linehan, J. C.; Schmid, B.; Autrey, T. *Phys. Chem. Chem. Phys.* **2007**, *9* (15), 1831–1836. doi:10.1039/b617781f. PMID:17415495.
(4) Hu, M. G.; Geanangel, R. A.; Wendlandt, W. W. *Thermochim. Acta* **1978**, *23* (2), 249–255. doi:10.1016/0040-6031(78)85066-7.
(5) Sit, V.; Geanangel, R. A.; Wendlandt, W. W. *Thermochim. Acta* **1987**, *113* (1), 379–382. doi:10.1016/0040-6031(87)88340-5.
(6) Wolf, G.; Baumann, J.; Baitalow, F.; Hoffmann, F. P. *Thermochim. Acta* **2000**, *343* (1-2), 19–25. doi:10.1016/S0040-6031(99)00365-2.
(7) Jaenicke-Rossler, K.; Leitner, G. *Thermochim. Acta* **2002**, *391* (1-2), 159–168. doi:10.1016/S0040-6031(02)00173-9.
(8) Baumann, J.; Baitalow, E.; Wolf, G. *Thermochim. Acta* **2005**, *430* (1-2), 9–14. doi:10.1016/j.tca.2004.12.002.
(9) Stephens, F. H.; Pons, V.; Tom Baker, R. *Dalton Trans.* **2007**, (25): 2613–2626. doi:10.1039/b703053c. PMID: 17576485.
(10) Haaland, A. *Angew. Chem. Int. Ed. Engl.* **1989**, *28* (8), 992–1007. doi:10.1002/anie.198909921.
(11) Klooster, W. T.; Koetzle, T. F.; Siegbahn, P. E. M.; Richardson, T. B.; Crabtree, R. H. *J. Am. Chem. Soc.* **1999**, *121* (27), 6337–6343. doi:10.1021/ja9825332.
(12) Thorne, L. R.; Suenram, R. D.; Lovas, F. J. *J. Chem. Phys.* **1983**, *78* (1), 167. doi:10.1063/1.444528.
(13) Kathmann, S. M.; Parvanov, V.; Schenter, G. K.; Stowe, A. C.; Daemen, L. L.; Hartl, M.; Linehan, J.; Hess, N. J.; Karkamkar, A.; Autrey, T. *J. Chem. Phys.* **2009**, *130* (2),o. 024507. doi:10.1063/1.3042270. PMID:19154038.
(14) Hughes, E. W. *J. Am. Chem. Soc.* **1956**, *78* (2), 502–503. doi:10.1021/ja01583a074.
(15) Shore, S. G.; Parry, R. W. *J. Am. Chem. Soc.* **1955**, *77* (22), 6084–6085. doi:10.1021/ja01627a103.
(16) Hoon, C. F.; Reynhardt, E. C. *J. Phys. Chem.* **1983**, *16* (32), 6129–6136. doi:10.1088/0022-3719/16/32/007.
(17) Demaison, J.; Liévin, J.; Császár, A. G.; Gutle, C. *J. Phys. Chem. A* **2008**, *112* (19), 4477–4482. doi:10.1021/jp710630j. PMID:18422295.
(18) Bowden, M. E.; Gainsford, G. J.; Robinson, W. T. *Aust. J. Chem.* **2007**, *60* (3), 149. doi:10.1071/CH06442.
(19) Hess, N. J.; Bowden, M. E.; Parvanov, V. M.; Mundy, C.; Kathmann, S. M.; Schenter, G. K.; Autrey, T. *J. Chem. Phys.* **2008**, *128* (3),o. 034508. doi:10.1063/1.2820768. PMID:18205511.
(20) Cho, H.; Shaw, W. J.; Parvanov, V.; Schenter, G. K.; Karkamkar, A.; Hess, N. J.; Mundy, C.; Kathmann, S.; Sears, J.; Lipton, A. S.; Ellis, P. D.; Autrey, S. T. *J. Phys. Chem. A* **2008**, *112* (18), 4277–4283. doi:10.1021/jp7117696. PMID:18407708.
(21) Taylor, R. C.; Cluff, C. L. *Nature* **1958**, *182* (4632), 390–391. doi:10.1038/182390a0.
(22) Custelcean, R.; Dreger, Z. A. *J. Phys. Chem. B* **2003**, *107* (35), 9231–9235. doi:10.1021/jp035267+.
(23) Sawodny, W.; Goubeau, J. *Z. Phys. Chem. (Frankfurt)* **1965**, *44*, 227.
(24) Dillen, J.; Verhoeven, P. *J. Phys. Chem. A* **2003**, *107* (14), 2570–2577. doi:10.1021/jp027240g.
(25) Allis, D. G.; Kosmowski, M. E.; Hudson, B. S. *J. Am. Chem. Soc.* **2004**, *126* (25), 7756–7757. doi:10.1021/ja048215m. PMID:15212505.
(26) Trudel, S.; Gilson, D. F. R. *Inorg. Chem.* **2003**, *42* (8), 2814–2816. doi:10.1021/ic026275s. PMID:12691593.
(27) Hemley, R. J.; Mao, H. K. *In High-Pressure Phenomena*, Proceedings of the International School of Physics Enrico Fermi, Vol. 147; Hemley, R. J., Chiarotti, G.L., Bernasconi, M., Ulivi, L., Eds.; IOS Press: Amsterdam, 2002; p. 3.
(28) Lin, Y.; Mao, W. L.; Drozd, V.; Chen, J. H.; Daemen, L. L. *J. Chem. Phys.* **2008**, *129* (23),o. 234509. doi:10.1063/1.3040276. PMID:19102540.
(29) Mao, H. K.; Xu, J.; Bell, P. M. *J. Geophys. Res.* **1986**, *91* (B5), 4673–4676. doi:10.1029/JB091iB05p04673.
(30) Smith, J.; Seshadri, K. S.; White, D. *J. Mol. Spectrosc.* **1973**, *45* (3), 327–337. doi:10.1016/0022-2852(73)90205-1.
(31) Jagielska, A.; Moszynski, R.; Piela, L. *J. Chem. Phys.* **1999**, *110* (2), 947. doi:10.1063/1.478139.